QoS Provisioning by Power Control for Video Communication via Satellite Links

Ting Ma[1][*][†], Yee Hui Lee[1], Stefan Winkler[2] and Maode Ma[1]

[1] *School of Electrical and Electronic Engineering, Nanyang Technological University, Singapore 639798*
[2] *Advanced Digital Sciences Center, University of Illinois at Urbana-Champaign, Singapore 138632*

SUMMARY

Video transmissions over satellite links are sensitive to signal fades due to rain, especially in the tropics. We performed a video streaming experiment over a satellite link for 24 days distributed over one year to investigate the effects of rain fade. Based on the measurements, models for the relationships between rainfall rate, power level, packet loss, and video quality are proposed. Furthermore, for both uplink and downlink channel, an adaptive closed loop power control algorithm, with a Proportional-Integral-Derivative (PID) controller is designed. This is used for the mitigation of the rain-induced attenuation in order to guarantee a certain level of Quality of Service (QoS) and Quality of Experience (QoE). Simulation results show the effectiveness of the proposed power control solution and its ability to sustain video quality levels in spite of rain fades. Copyright © 2014 John Wiley & Sons, Ltd.

KEY WORDS: Ka-band satellite; video streaming quality; power control; PID controller

1. INTRODUCTION

Satellite multimedia communications play a significant role in our daily life because of their ability to deliver services to a large number of customers over a wide area, even in remote locations where there are no terrestrial connections. There is an overwhelming trend towards the use of satellite communication services for digital video delivery in recent years. Geostationary Earth Orbit (GEO) satellite systems have been used for many years in long distance broadcasting [1]. For broadcasting applications, a typical example is Digital Video Broadcasting (DVB) that implements bi-directional DVB Return Channel by Satellite (DVB-RCS) standards [2] to deliver television services to consumers. For real time interactive communications, two or more geographically separated local area networks can be interconnected via satellite links using the Internet Protocol (IP), which supports various multimedia services such as video conferencing and voice over IP (VoIP) [3]. Delay-sensitive real-time multimedia applications usually adopt user datagram protocol (UDP) [4]. The real-time transport protocol (RTP) at the application layer that supports various types of codecs is responsible for end-to-end real-time service of streaming traffic by providing timely delivery of content to the applications [5].

The lower frequencies used for commercial satellite communications, like C-band (4-8 GHz) and Ku-band (12-18 GHz), have become congested. Therefore, higher frequency bands, such as the Ka-band (approximately 20-30 GHz), are attracting growing interest for both commercial and military satellite operators. However, the disadvantage of the Ka-band is its vulnerability to signal attenuation under certain weather conditions, in particular rain [6,7]. Rain attenuation is more severe in the tropical region where heavy

---

[*]Correspondence to: Ting Ma, School of Electrical and Electronic Engineering, Nanyang Technological University, Singapore.
[†]E-mail: mati0004@e.ntu.edu.sg

convective rain dominates [8]. This high rain attenuation cannot be overcome simply by system margins. Rain-induced fades can cause significant propagation loss to satellite communication systems operating at frequencies above 10 GHz, with attenuations of over 20 dB at 100 mm/hr rainfall rate [9]. The effects of rain on radio-wave propagation become more severe as the frequency increases. Along with the degradation of the received radio-wave signal, the signal to noise ratio worsens, leading to a higher packet loss rate. Therefore video services are inevitably affected by rain attenuation.

Various rain fade mitigation techniques have been proposed in order to maintain the QoS requirements for multimedia applications. In general, there are three rain fade countermeasures for satellite broadcast systems: time diversity, site diversity, and power control. The common advantage of these three techniques is that they do not impose the burden of extra bandwidth allocation, in contrast with digital processing methods such as adaptive modulation or variable symbol rate [10].

- Time diversity is the retransmission of a signal several times with an acceptable delay. The receiver selects the best quality signal out of all accumulated received ones [11]. However, the time diversity technique is confined to delay-insensitive services.
- Site diversity takes advantage of the fact that if the signal is heavily attenuated by a rain cell in one area, there will be other ground stations spatially separated that are unaffected by the same rain cell and can be used to compensate. Site diversity requires two or more stations that are spatially far enough apart to be capable of improving overall system performance [12]. The diversity gain depends on geographical site separation, elevation angle, and other factors. The disadvantages of this technique are the cost of setting up additional sites and the requirement for data buffering.
- The power control approach aims at maintaining a desired received signal level by varying the power of the transmitter. This is one of the simplest, most commonly used and most efficient rain attenuation mitigation techniques available, and will be explored in this paper.

Several power management schemes have been proposed for wireless video service in code-division multiple-access (CDMA) systems [14,15]. In such a system, the bit-error-rate (BER) is adjusted by controlling the transmitter power according to the importance of each video packet. In satellite communication systems, Dennis et al. have proposed a scaling uplink power control algorithm for satellite systems working in the 30/20-GHz band [16]. The proposed algorithm makes use of 20 GHz attenuation scaled to 30 GHz to adjust the transmitted power at 30 GHz. The drawback of this scheme is that the dynamic range of power control is limited to approximately 10-12 dB. Another adaptive transmission power control scheme using a multi-beam satellite antenna is presented in [17]. In this scheme, the transmission power of the transmitter from the satellite towards the targeted site is controlled according to the attenuation at the reference sites. This scheme is only suitable for communication systems where the distance between sites is small; if the distance is large, this scheme produces little performance improvement. Although there are some other solutions for satellite transmission with power control techniques [18-19], none of them have provided insights into high quality video transmission over satellite links.

In this paper, the effects of rain-induced attenuation on real-time video streaming via a Ka-band satellite link are examined. The focus of our analysis is on the correlation between rainfall rate, video quality and power level. Based on the correlation between these parameters, two numerical models are derived, relating (a) the rainfall rate with the received power level, and (b) the rainfall rate with the IP packet loss rate. Using these models, an effective adaptive power control technique for rain attenuation mitigation is proposed. The main contributions of this paper can be summarized as follows.

1) The statistical relationships between rain attenuation and received signal level, packet loss rate, and video quality are presented. These relationships are based on experimental results obtained from a real-time video transmission via satellite link.
2) The analytical models for rainfall rate versus IP packet loss rate and rainfall rate versus received power level are derived.
3) A PID controller that uses an adaptive closed loop power control approach in both uplink and downlink

is proposed to overcome rain attenuation for video streaming via Ka-band satellite links.

4) The effectiveness of our proposed scheme is verified using simulations.

The paper is organized as follows. Section 2 describes the configuration of the real-time video streaming system. The detailed process of video streaming and video quality metrics are also presented. In Section 3, the numerical results obtained experimentally are analyzed and discussed, based on which models of rain effects on video streaming over satellite links are derived. The adaptive power control algorithm with PID controller is presented in Section 4. Simulation results to demonstrate the effectiveness of the proposed algorithm are also presented. Conclusions are drawn in Section 5.

2. VIDEO STREAMING SYSTEM

As shown in Figure 1, the video streaming system is composed of a video server and a video receiver, both of which communicate via the Wideband Inter-Networking engineering test and Demonstration Satellite (WINDS) using ultra-small aperture terminals (USAT). WINDS was launched by the Japan Aerospace Exploration Agency (JAXA) and the National Institute of Information and Communications Technology (NICT) in February 2008. WINDS aims to develop technologies for ultra-high data rate satellite communications in the Ka-band [20]. The USAT with a two reflector antenna is an earth station developed for easy deployment and installation in inaccessible areas for communication purposes. A significant characteristic of the USAT is its ability to provide high-speed communication at a downlink rate of 155Mbps using an ultra-small reflector antenna with a diameter of only 45cm [21]. The indoor unit (IDU) in our system provides time division multiple access (TDMA) synchronization, data modulation and demodulation. In transmission mode, the IDU implements code modulation for the data on the Ethernet interface from the user equipment and passes it on to the outdoor unit (ODU) which is responsible for converting the intermediate frequency (IF) signals to radio frequency (RF) signals and vice versa (Figure 1).
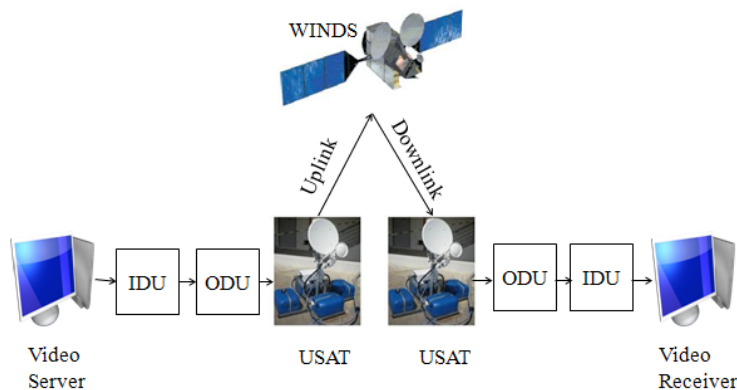

Figure 1. Video Transmission via WINDS.

2.1. Video streaming

A loopback transmission mode is adopted in our experiment to investigate the characteristics of video communication via satellite. The content is transmitted from our site via the uplink to WINDS and received back at the same site via the downlink. WINDS acts as a bent pipe, receiving and then re- transmitting back to the same site. If the transmission suffers rain fades, both the uplink and the downlink are affected. In this paper, the measured two-way loss rate is referred to as IP packet loss rate.

For satellite transmissions, a video codec with high compression efficiency is required. We choose H.264/MPEG-4 Advanced Video Coding (AVC) for our experiments [22]. Considering the maximum raw

data rate of approximately 4.96 Mbps on the loopback link, the video is compressed to 3.5 Mbps to leave sufficient room for packetization and other overheads. After encoding, the video elementary stream is multiplexed into an MPEG2 transport stream (TS) using the tsMuxeR software [23]. The IP packets of a streaming session with a direct PC-to-PC link are recorded using tcpdump [24] into a packet capture (PCAP) file for consistent repeatable playback and post-processing.

In our real-time video streaming experiments, tcpreplay [24] is adopted to play back the PCAP files at the video server over the WINDS links in a continuous loop. The client side runs tcpdump to log the network traffic and capture the arriving video packets in PCAP format. Post-processing and analysis is then performed on the PCAP files in order to extract various quantifiable parameters from the captured files, such as the packet loss rate and video quality.

2.2. Video quality measurement

Losses of the satellite signal due to rain attenuation will directly affect the transmitted bit stream. The resulting errors will be observed as packet loss at the receiver end. Thus, packet loss will be taken into consideration throughout the following analysis. However, packet loss alone is not a reliable indicator of video quality, because of the complexities of video signals as well as the human visual system.

For a more accurate assessment of video quality, objective and subjective approaches can be employed. Subjective video quality evaluation is concerned with how video is perceived by a viewer and his or her opinion of a particular video sequence [25]. The mean opinion score (MOS) is usually adopted to assess perceived quality in subjective video evaluation. Being time-consuming and cumbersome are the main drawbacks of subjective video quality assessment, especially when it involves hundreds of hours of continuous video monitoring as in our experiments. Objective video quality evaluation techniques on the other hand use mathematical models to estimate the quality of a video as perceived by the human eye. Most image processing studies only implement basic objective quality measurements such as the peak signal to noise ratio (PSNR) and mean squared error (MSE). However those are not only unreliable but also impractical for measuring the quality of streaming video [26].

In this paper, we apply the hybrid V-Factor metric [27] to measure video quality. The V-Factor metric is based on deep packet inspection of the video stream. It takes into account not only the impact of network impairments, like jitter, delay and packet loss, but also the impact of video impairments due to the content characteristics, the compression mechanism and bandwidth constraints. The value of V-Factor ranges from 1 (bad) to 5 (excellent) in accordance with MOS.

3. MODELING RAIN EFFECTS ON SATELLITE LINKS

3.1. Rain data

Data was collected in video streaming experiments conducted over two days each month for an entire year. Two common types of rain events, namely convective rain and stratiform rain, have been observed during our experiments. *Stratiform rain* has a relatively low rainfall rate of less than 25 mm/hr, and generally lasts for a longer period of time. The rainfall rates of *convective rain* on the other hand exceed 25 mm/hr, but these events typically last for a short period of time.

Figure 2(a) depicts the data collected from May 20th to 21st, 2010 as an example. A stratiform rain event with up to 6 mm/hr of rainfall rate at around 17 hours into the experiment was recorded. This stratiform rain event lasted for a period of over 4 hours. This rain event resulted in a power level drop of up to 5 dB and an IP packet loss rate of up to 4%. The V-Factor occasionally drops to 1 throughout the rain event.

Figure 2(b) shows another data set collected from June 21st to 22nd, 2010. An obvious convective rain event with up to 60 mm/hr occurred at around 9 hours into the experiment, which caused signal levels to drop by approximately 17 dB. Unlike the stratiform rain event, this convective rain event lasted for only 40 minutes and led to nearly 100% IP packet loss and unacceptable video quality (V-Factor of 1) for the entire duration of the rain event.

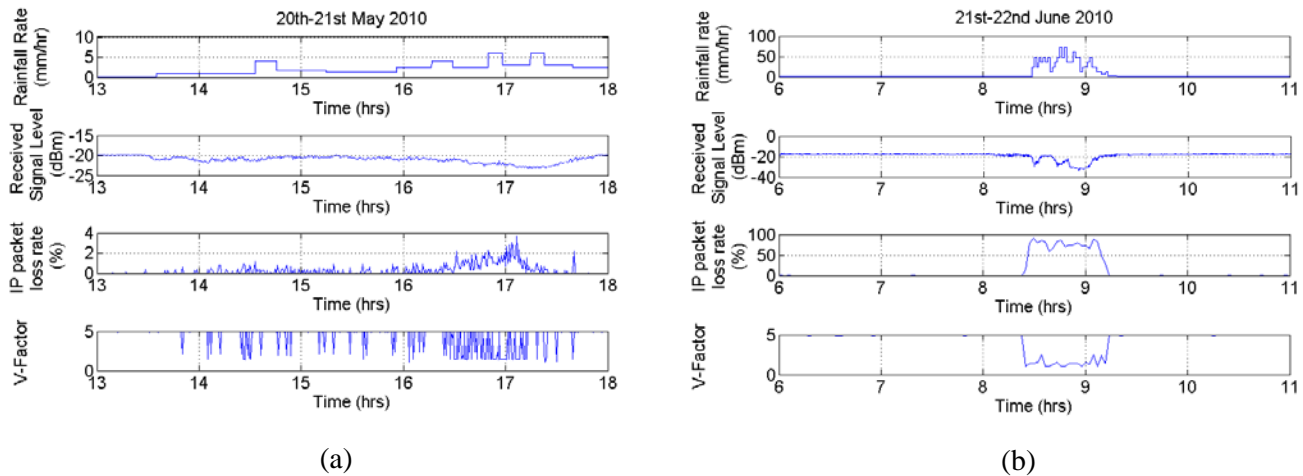(a)   (b)

Figure 2. Rainfall rate, IP packet loss and V-Factor for (a) stratiform and (b) convective rain events.

From the measurements, it can be seen that the rainfall leads to a decline in signal level and an increase in IP packet loss rate. To quantify the impact of rain fades on both received signal level and IP packet loss rate, the measurement results were used to model the relationships by means of least mean squares curve-fitting. Note that all the data points used in the following figures for data fitting are derived from the data of the whole measurement campaign.

3.2. Rainfall rate and signal level

Figure 3 shows a plot of the signal level versus the rainfall rate. From the depicted behavior, the received signal level decreases exponentially with the increase of rainfall rate, which can be modeled with the following function:

$$P = 16.57 * e^{-0.04363*r} - 33.57 \tag{1}$$

where r represents the rainfall rate, and P is the received signal level. The signal level initially drops fast until its deterioration saturates after the rainfall rate reaches 24 mm/hr.
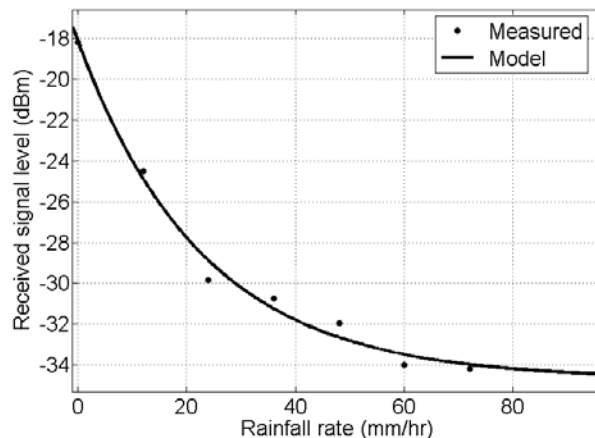

Figure 3. Signal level vs. rainfall rate (measured data and model).

The prediction model defined in ITU-R P.618 have been developed to calculate rain attenuation [28]. This model can estimate long-term statistics of the slant-path rain attenuation at a given location for frequencies up to 55 GHz. Therefore, a comparison between the proposed model and the ITU-R model will be performed

here.

The ground station USAT is located at Singapore (1.34ºN, 103.68º) with an elevation angle of 45º. The specific attenuation γ_R can be obtained using the frequency-dependent coefficients given in Recommendation ITU-R P.838 [29] and the rainfall rate exceeded 0.01% of time, $R_{0.01}$:

$$\gamma_R = k\left(R_{0.01}\right)^{\alpha} [dB/km] \tag{2}$$

The effective slant path length L_E is calculated using the elevation angle, latitude, and rain height (refer to [28] for details). The attenuation exceeding 0.01% of the year $A_{0.01}$ is calculated as follows.

$$A_{0.01} = \gamma_R L_E [dB] \tag{3}$$

Finally, the estimated attenuation to be exceeded for other percentages p of an average year, in the range 0.001% to 5%, can be derived from $A_{0.01}$ as follows:

$$A_p = A_{0.01}\left(\frac{p}{0.01}\right)^{-\left(0.655+0.033\ln(p)-0.045\ln\left(A_{0.01}\right)-\beta(1-p)\sin\theta\right)} \tag{4}$$

where θ is the elevation angle (in degrees), and $\beta=0$ when $p\geq1\%$ in our case.

Since the ITU-R model is a widely accepted rain attenuation prediction model, a comparison between the ITU-R model and our proposed model (1) is made. Figure 4 depicts the cumulative distribution functions (CDFs) of rain attenuation based on both models in comparison with our measurements. It can be observed that the predicted rain attenuation is within close range for both models and is consistent with the measured attenuation. Besides, the general attenuation trends for both models are similar and resemble the real situation. In conclusion, the comparison indicates that the proposed model fits the measured data well and is also consistent with the ITU-R model. The proposed model is not complex, as it consists of a simplified exponential function, whereas the ITU-R model involves solving a series of complex equations. Therefore, our model has the advantage of wide prediction range and simplicity.
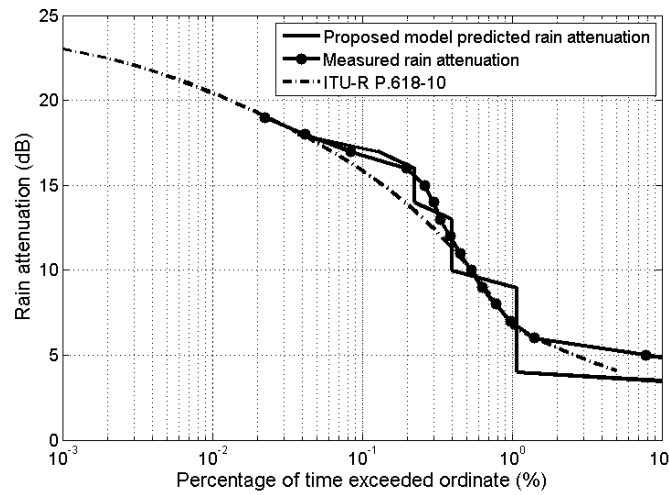

Figure 4. CDF comparison of predicted and measured rain attenuation.

3.3. Rainfall rate and IP packet loss

Next, the relationship between rainfall rate and IP packet loss is derived from the measured data. The relationship between the rainfall rate r and the IP packet loss L can be modeled as follows (Figure 5):

$$L = 49.83 * \tanh\left(\frac{r-38.7}{16.981}\right) + 48.7961 \tag{5}$$
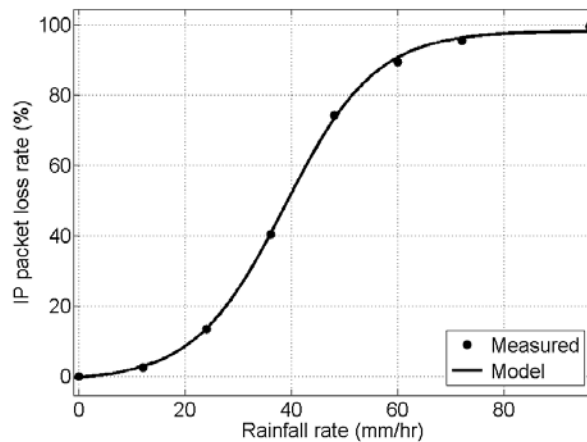
Figure 5. IP packet loss as a function of rainfall rate (measured data and model).

Furthermore, the mathematical relationship between the received power level and IP packet loss rate can be derived from (1) and (5).

First of all, the rainfall rate can be expressed in terms of the received power level P:

$$r = \frac{In\dfrac{P+33.57}{16.57}}{-0.04363} \tag{6}$$

given the mathematical property of

$$\tanh = \frac{e^x - e^{-x}}{e^x + e^{-x}} \tag{7}$$

we can obtain the direct correlation between received power level and IP packet loss:

$$L = 49.83 * \frac{20.5529*(P+33.57)^{-2.6996} - 1}{20.5529*(P+33.57)^{-2.6996} + 1} + 48.7961 \tag{8}$$

The measured data and the modeled relationship in (8) between the received power level and the IP packet loss is depicted in Figure 6. As shown, the proposed model closely fits the measurements. The IP packet loss rate increases with declining received signal level.

Table 1 shows the numerical quality of the model fits in terms of root mean squared error (RMSE) of the residuals and R-squared. The RMSE measures the difference between predicted value and actual value. The R-squared indicates the quality of fit of the model, where a value of 1 indicates perfect agreement between predicted and observed values.
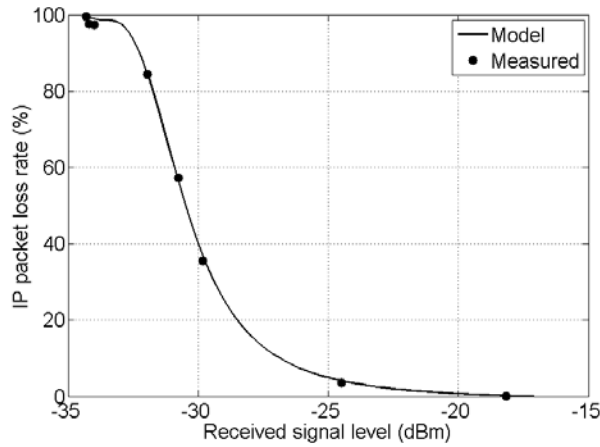
Figure 6. IP packet loss rate as a function of received signal level (measured data and model).

Table I. Evaluation of model fitting.

Evaluation metric	Received power versus rainfall rate (Eq.1)	IP packet loss versus rainfall rate (Eq.5)	IP packet loss versus received power (Eq.8)
RMSE	0.51 dBm	0.90 %	1.22 %
R-squared	0.9908	0.9995	0.9990

The RMSE or our proposed fitted models is low and R-square values are very close to one, therefore all three models provide excellent fits to the measured data.

In order to verify these results, CDFs of the received power and IP packet loss rate over one-year experimental days are calculated by applying the fitting models to the full one year rainfall data. Comparisons between the model predictions and the measured data are shown in Figure 7 and Figure 8. In general, there is a very good agreement between the two. The major advantage of the demonstrated correlation is that, based on a given rainfall rate, predictions of the received signal level and IP packet loss rate can be obtained. This allows us to implement an effective power control scheme using the proposed models.
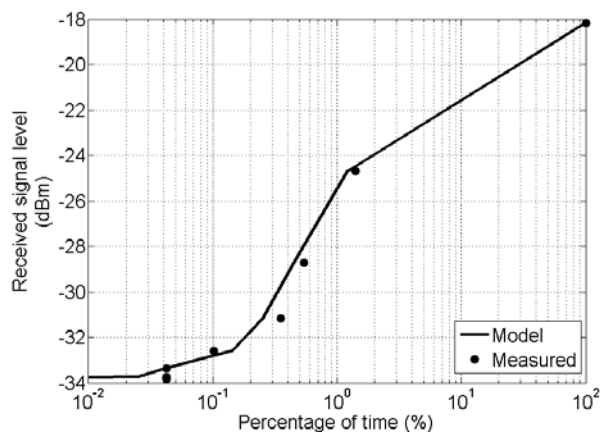

Figure 7. CDF comparison of predicted and measured received signal level.
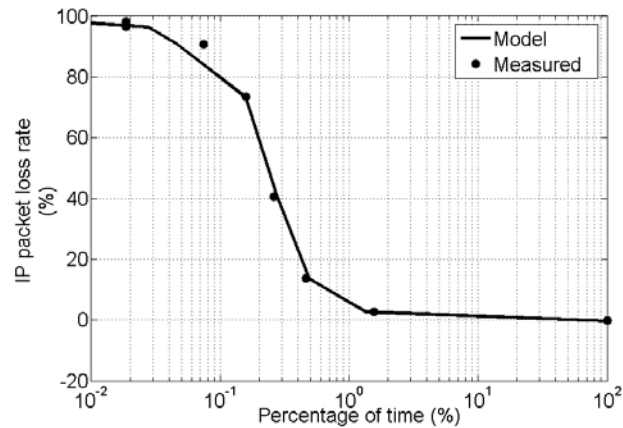
Figure 8. CDF comparison of predicted and measured IP packet loss rate.

Since there is a close relationship between IP packet loss rate and video quality, we need to determine the maximum acceptable IP packet loss rate that will produce a video quality that is still acceptable to viewers. In order to better demonstrate the relationship between IP packet loss rate and V-Factor, we have compiled all the experimental data together. The V-Factor is shown as a function of IP packet loss rate in Figure 9. V-Factor exhibits a sharp step function, which shows that a V-Factor of 3 or above (indicating acceptable or better video quality) can be achieved when the IP packet loss is below 1%. The V-Factor drops below 1.5 (indicating unacceptable video quality) when the IP packet loss goes above 1%. Consequently, 1% IP packet loss rate has to be maintained to guarantee acceptable video quality. For the purpose of our experiments, the IP packet loss rate is therefore the major parameter that will be analyzed for our proposed power control scheme.
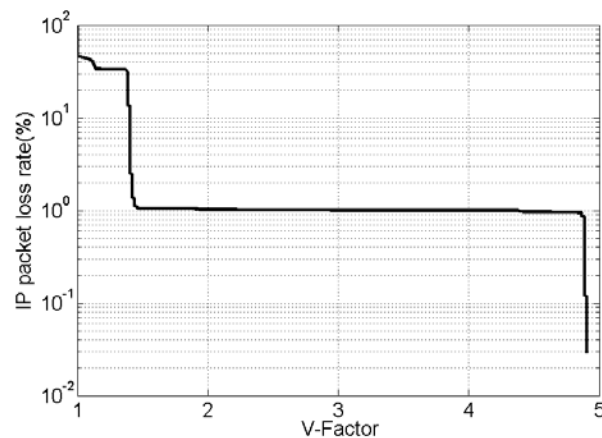

Figure 9. Relationship between the IP packet loss rate and V-Factor.

4. POWER CONTROL ALGORITHM

As shown in the previous section, video quality is largely dependent on IP packet loss, which in turn is determined by received signal strength. Therefore, in order to guarantee an acceptable video quality under different rainfall rate conditions, the transmit power has to be adjusted to compensate for losses. Conventional schemes like uplink power control or downlink power control are based on adjusting either the earth station transmitting power or satellite transponder gain. Those methods working alone suffer from latency caused by long round trip delay. Furthermore, the required compensation power or gain becomes a

serious burden when either the satellite transponder or earth station is working alone under power control, which may easily push them to their power limits.

In this paper, we have combined uplink and downlink power control schemes to propose an adaptive closed loop power control algorithm with Proportional-Integral-Derivative (PID) controller. PID controllers have been widely adopted in systems with feedback to efficiently achieve stabilized state [30-31]. As weather conditions are always changing, a closed loop feedback power control system is needed to achieve the aforementioned compensation of the transmitting power. The benefit of a closed-loop power control approach is that it is able to adjust the transmission power adaptively according to current weather conditions in real time. In addition, a PID controller can help smoothen the feedback process, especially under drastic changes in rainfall rates. The proposed adaptive power control mechanism is designed to adjust both the satellite and earth station transmitting power in accordance to the commands generated by comparing the target and measured received signal level. Due to the contributions from both satellite and earth station, the loop is expected to react more quickly to the adjusting commands, which reduces the system stabilization time. Moreover, both satellite transponder and earth station share the responsibility to supply the required power compensation. Therefore, problems due to power limitation will be alleviated as well.

4.1. Simulation model

To verify the effectiveness of the proposed adaptive power control scheme, simulations are carried out using MATLAB Simulink. Figure 10 shows the simulation model in the form of a block diagram for the proposed scheme. There are five main model components in the simulation system: Earth Station, Uplink Channel, Satellite Transponder, Down-Link Channel and Rain Event.

$T_{rb}(t)$: Base Station Transmitting Power
$C_s(t)$: Command for Satellite
$R_{rs}(t)$: Satellite Received Power
$T_{rs}(t)$: Satellite Transmitting Power
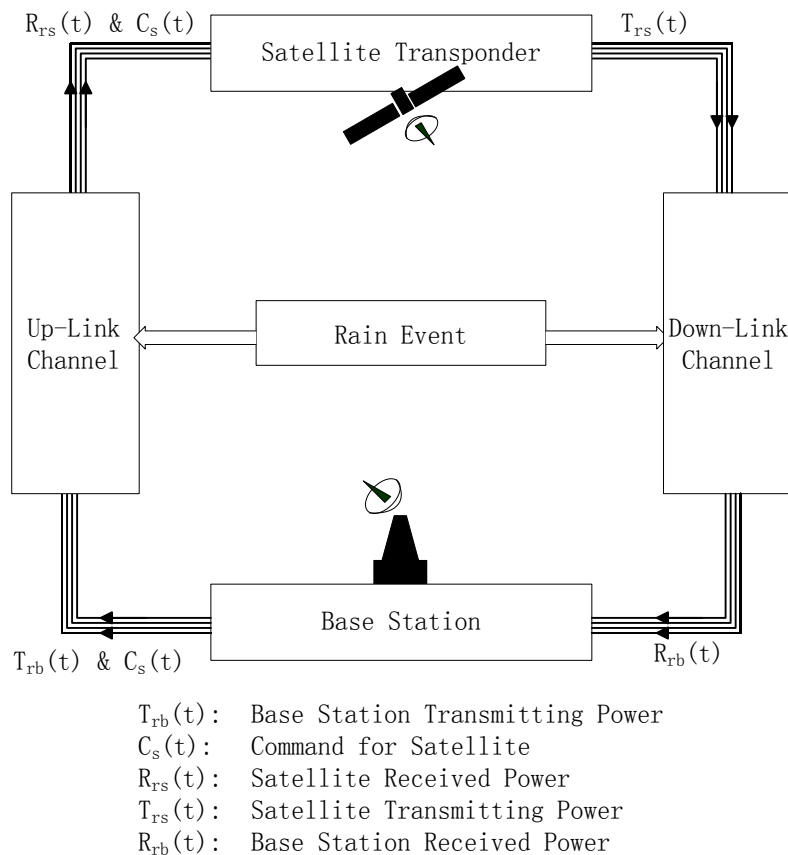$R_{rb}(t)$: Base Station Received Power

Figure 10. Block diagram of the proposed adaptive power control system.

The Earth Station receives the signal from the satellite. After proper calculation, it generates an adjusted transmit signal and power control command to the satellite. This calculation process is performed in the major compensation controller inside the Earth Station. It takes a target received signal power as a reference level and computes the current difference between the actual received signal power level and the reference level. This difference is considered as the instantaneous compensation power. However, directly injecting this difference as compensation power into the power control system can easily cause the system to become unstable. Therefore, a properly designed PID controller is added. The output of the PID controller is then taken as the total required compensation power. With proper weights, the total required compensation power is split into two parts; one to control the Earth Station transmitting power; and the other to control the Satellite Transponder gain. The command for the Earth Station is carried out instantly, and the adjusted transmitting power is generated, while the command for Satellite is then coded and sent to the Satellite via the transmission channel.

According to the power control command, the Satellite transponder tunes its gain to amplify the received attenuated signal to be sent back to the Earth Station.

The Rain Generator block generates different real-time rainfall rates to the up/down link channels to simulate rain effects on the satellite links.
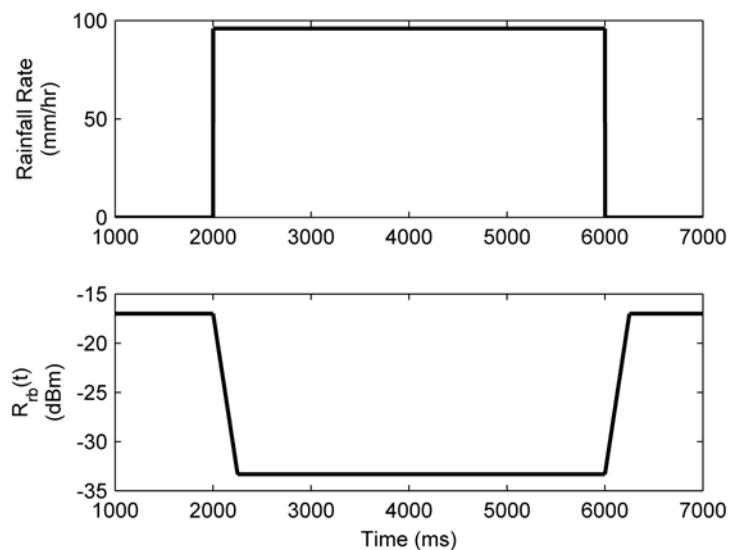

Figure 11. Simulation of the system without power control in a rain event.

The Up-Link and Down-Link Channels are properly modeled to include the propagation loss and rain attenuation loss. The round trip delay is split equally between the Up-link Channel block and the Down-Link Channel block, so that each of them has 125 ms delay. In order to improve the accuracy of the model, the channel model block is designed to have a 1ms resolution. This setting accounts for two facts. Firstly, due to the round trip delay, the receiving signal power still suffers from the rain attenuation within a short period after the rain event stops; secondly, when the rain starts, the signals along the transmission path experience different levels of rain attenuation: the closer the signal is to the receiving block, the less rain attenuation it will suffer.

A simulation of a simple case with a pulse rain event without compensation is shown in Figure 11. As can be clearly seen, after the end of the rain event at 6000 ms, the received signal power level gradually recovers to its normal level without abruptly changing state. This result resembles the real situation more closely.

4.2. PID controller parameters

Due to time delays in the loop, the outdated feedback information can result in a dynamic behaviour, which may lead to oscillations at the response side. A properly tuned PID controller should reach stability in the shortest settling time. In [32,33], PID controllers are studied in a closed-loop control system with propagation delay. A generalized representation of the PID controller can be written as:

$$C(t) = K_p * e(t) + K_i \int_0^t e(t)dt + K_d \frac{de(t)}{dt} \tag{9}$$

where $e(t)$ represents the error signals, and K_p, K_i and K_d are proportional gain, integral gain, and derivative gain, respectively. The proportional term of the PID controller is responsible for the output that is proportional to the current error. The proportional gain cannot be too high, otherwise the system will become unstable. At the same time, the proportional gain cannot be too low, or the control action will become too small when responding to a disturbance. The typical function of the integral action is to eliminate offsets of the steady state and to guarantee that the output agrees with the target value in a steady state. The derivative term is a prediction of future errors, based on the current rate of change. The derivative term is highly sensitive to noise in the error term and may cause the PID controller to go into an unsteady state if the noise and K_d are sufficiently large.

In our system, the receiving power level is sampled at discrete time intervals with a sampling period of T. The PID controller in equation (9) is thus modified as:

$$C(kT) = K_p e(kT) + K_i T \sum_{n=0}^k e(kT) + K_d \frac{e(kT) - e[(k-1)T]}{T} \tag{10}$$

A heuristic method proposed by Ziegler and Nichols is adopted to tune the PID parameters to achieve the desired performance for the whole power control system [34]. The step response of the whole system with rain event as its input is investigated. Note that the rain event is assumed as a square pulse which has a step rising edge and a step falling edge. The purpose is to fully evaluate the system with a more realistic rain environment. The sampling time T is set to 1 ms for the PID controller tuning process.

According to Ziegler and Nichols' method, initial values of the parameters are set to $K_i = K_d = 0$ and K_p is continuously increased to observe the system response. The responses are shown in Figure 12. It can be shown that merely increasing K_p will ultimately cause the whole system to oscillate. It is also observed that the oscillation period remains the same when further increasing the proportional gain higher than 1. Thus the ultimate gain of the PID controller would be $K_p = 1$. The oscillation periods are the same (500 ms) for all values of K_p.

The next step of the PID controller parameters tuning will be the integral gain K_i and differential gain K_d. As a common practice, the differential gain can be set to zero to reduce the chance of potential instability. Thus the response of the base station receiving power is reported in Figure 13 with different K_i settings. Also in line with the prediction of Ziegler and Nichols' method, Figure 13 indicates that higher integral gain K_i can improve the settle time of the closed loop system. However, continuously increasing K_i cannot completely eliminate the settle time. This is because of the intrinsic round trip delay associated with the satellite communication system. The delay postpones the system's reaction to any adaptation command. In fact, even with a perfectly tuned PID controller, the minimum settle time for the whole power control system should be no shorter than the round trip delay.
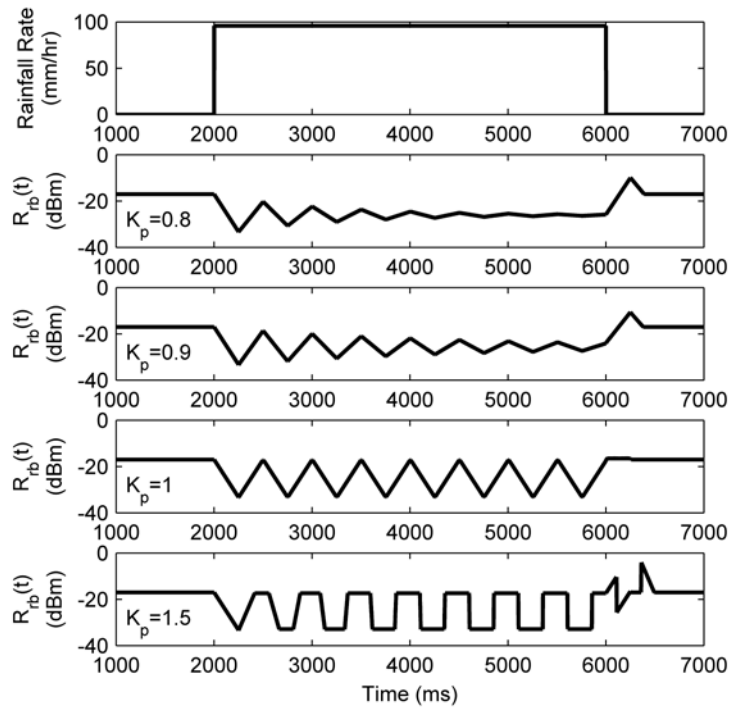
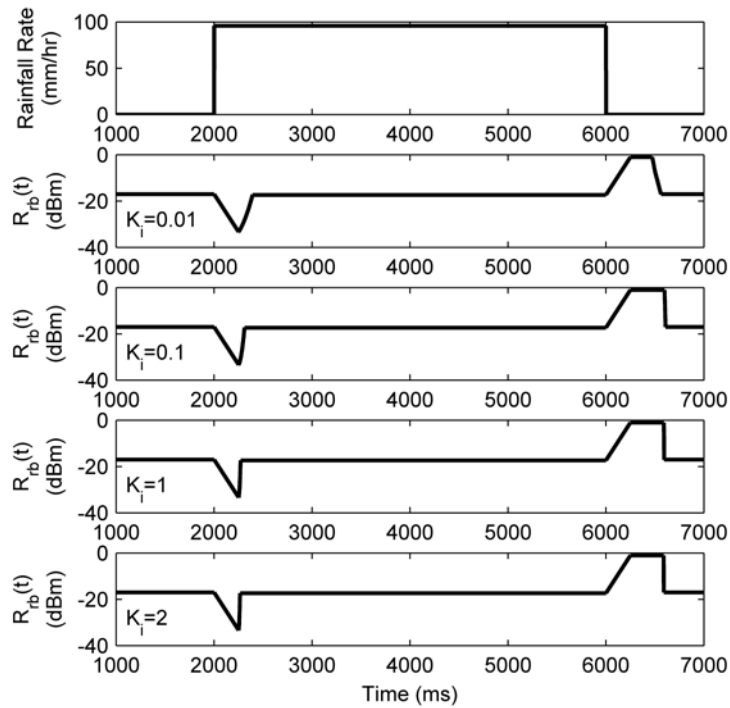Figure 12. PID parameter tuning: different K_p with $K_i=K_d=0$.

Figure 13. PID parameter tuning: different K_i with $K_p=1$ and $K_d=0$.

According to the simulation results, the proportional gain K_p can be set to a value higher than 1. An intuitive effect of a large K_p is that the calculated compensation power should be very high. However, in the proposed

control system, the maximum applicable compensation power is set to 8 dBm for both the base station and the satellite transponder. Furthermore, the compensation power level is considered as non-negative. This means the proportional gain K_p of the PID controller can be set as high as desired, because the actual compensated power is at most 16 dBm in total, and a high K_p benefits the performance with a more rapid adjustment for the whole system. As a result, we choose $K_p=1$, $K_i=1$ and $K_d=0$ for our control system.

As mentioned previously, the sampling time was chosen as 1 ms for the PID controller tuning. Due to the delay of the satellite system, the sampling time can be made longer. A comparison is shown in Figure 14 for $K_p=1$ and $K_i=K_d=0$. As can been seen, the oscillation amplitude and period are the same for the two cases. This indicates that a sampling time of 125 ms has no negative impact on the system compared to a sampling time of 1 ms. As a result, the final sampling time is chosen as 125 ms to alleviate the computational cost for the base station.
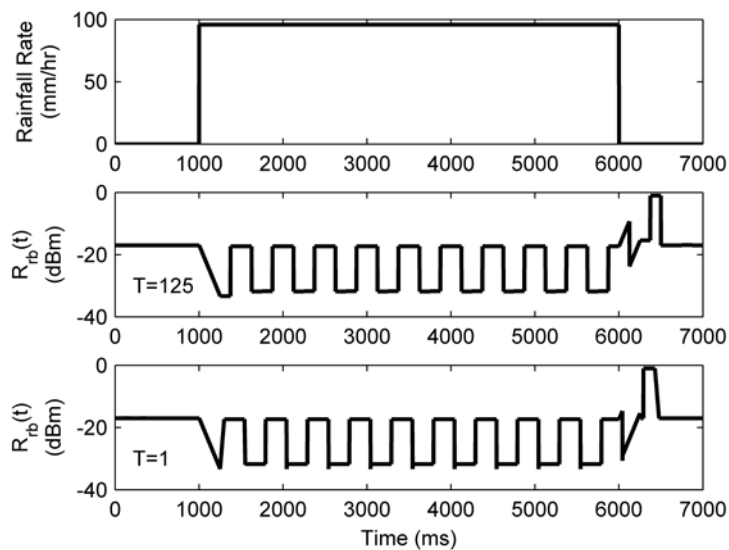

Figure 14. Comparison between different sampling times $T=125$ ms and $T=1$ ms with $K_p=1$, $K_i=K_d=0$.

In the scenario of multi base stations sharing a common satellite transponder, the power control can be performed at the spot beam level [35]. In addition, duplex techniques such as time division multiple access can also be used to allocate the satellite transponder for multi base stations. The sampling time T will be correspondingly larger.

4.3. Evaluation and results

In order to further evaluate the proposed scheme, the comparison of the system responses with and without power control implementation is presented in Figure 15. The rainfall rate is designed to increase gradually from 0 to 96 mm/hr which is the largest rainfall rate observed in our experiment records. The probability of rainfall rate exceeding 96 mm/hr is approximately 0.01% in one year, so 96 mm/hr effectively represents very heavy convective rain. The normal received signal level declines due to the rain attenuation. It is also demonstrated that the received signal level reduces as the rainfall rate continues to increase. Accordingly, the IP packet loss rate simultaneously goes up as a reaction to the decrease in received signal level. On the other hand, the received signal level with PID power control as a countermeasure shows that these effects can be well compensated, regardless of rainfall rate variations. The IP packet loss rate can be reduced to near zero, ensuring high video quality. The comparison demonstrates that the proposed PID power control technique can effectively improve the quality of the video transmission under rain attenuation.
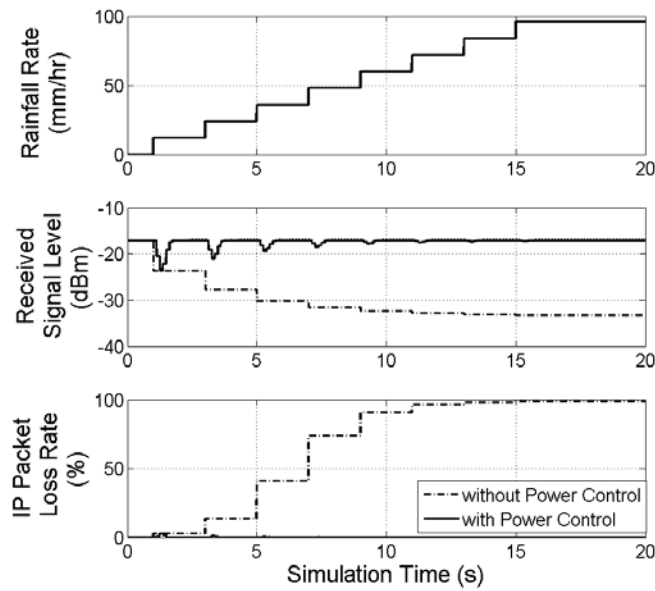
Figure 15. Comparisons of received signal level and IP packet loss responding to rainfall rate fluctuations with and without power control.

In addition, the performance of the proposed approach has been assessed using the full one year rainfall rate data collected with the weather station in 2010. In order to alleviate the non-linearity issue, the maximum total compensating power that the Earth Station and the Satellite transponder can provide together is assumed to be 10 dB. Figure 16 shows the CDF of IP packet loss rates for one year with and without the proposed power control. It can be observed that the link reliability has been significantly enhanced. The probability of IP packet loss rates below 1% is increased from 98.97% to 99.65% with the implementation of the power control technique. Over the duration of a whole year, this means the total amount of time with higher than 1% IP packet loss rate is reduced from 90.23 hours to 30.66 hours, i.e. the proposed power control scheme reduces the amount of video communication with unacceptable quality by a factor of 3. Therefore, it can be concluded that our power control scheme significantly improves the overall performance of the satellite link.
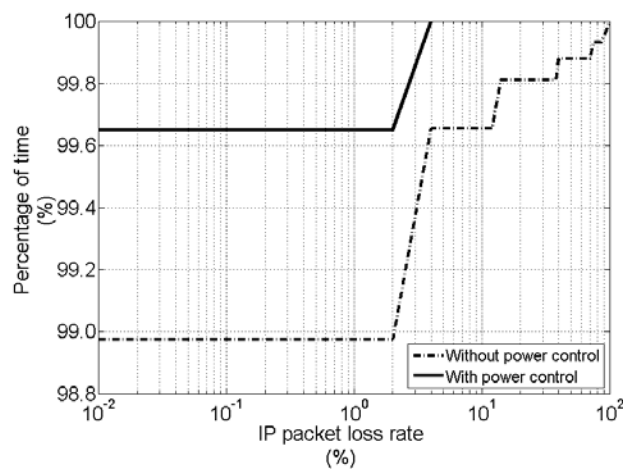

Figure 16. The CDF of IP packet loss rate of 2010 one-year rainfall data with and without power control.

4.4. Bitrate Adaptation

According to the previous simulation and analysis, a total compensation power of 16 dBm is needed in the case of maximum rain (96 mm/hr). This amount of extra power may not be affordable by the base station or satellite transponder. However, this problem can be alleviated by adapting the transmission data rate. The Shannon-Hartley theorem states that a noisy communication channel has a maximum capacity limit [36] and can be expressed as follows:

$$R = B\log_2(1 + \frac{S}{N_o B})$$
(11)

It indicates that, given a fixed bandwidth B and noise density N_o, a higher transmission power S is needed for a higher bitrate R data stream. This property makes it possible to trade off bandwidth efficiency for power level. In our case, it means that the compensation for the uplink and downlink power gain need not be too high when heavy rain occurs, because lowering the bit rate of the video transmission can improve the energy per bit to noise power density ratio (E_b / N_o) and thus enhance the bit error rate performance. An example based on the techniques with code and bitrate adaptation has been demonstrated in [37].

5. CONCLUSION

Video streaming over satellite links can be subject to severe signal degradations due to rain attenuation. A number of experiments of video streaming via satellite links have been conducted to investigate the relationships between four major factors: rainfall rate, received power level, IP packet loss, and video quality. Statistical analysis has been performed to extract these relationships. Three models for power level versus rainfall rate, IP packet loss versus rainfall rate and IP packet loss versus power level have been proposed and verified. Based on these relationships, a closed-loop adaptive power control scheme has been proposed as a countermeasure to overcome the degradation of video quality caused by rain fades. A PID controller was used to mitigate the settling time of the received signal strength towards the desired level. Simulation results have shown the effectiveness of the proposed power control scheme and its ability to maintain good video quality in spite of rain fades. The proposed power control scheme is able to improve the reliability of the satellite link by approximately 3 times based on the data for the year 2010.

ACKNOWLEDGMENTS

REFERENCES

1. F. De Rango, M. Tropea, P. Fazio and S. Marano. Call admission control for aggregate MPEG-2 traffic over multimedia Geo-satellite networks. *IEEE Trans. Broadcasting* 2008; **54**(3):612-622.
2. Digital Video Broadcasting (DVB): Interaction Channel for Satellite Distribution Systems, ETSI EN 301 790 v1.5.1, May 2009.
3. F. Filali, G. Aniba and W. Dabbous. Efficient support of IP multicast in the next generation of GEO satellites. *IEEE J. Sel. Areas Commun.* 2004; **22**(2):413-425.
4. H. Zheng and J. Boyce. An improved UDP protocol for video transmission over Internet-to-wireless networks. *IEEE Trans. Multimedia* 2001; **3**(3): 356-365.
5. G. Cunningham, P. Perry, J. Murphy and L. Murphy. Seamless handover of IPTV streams in a wireless LAN network. *IEEE Trans. Broadcast.* 2009; **55**(4): 796-801.

6. J. P. Choi and V. W. S. Chan. Predicting and adapting satellite channels with weather-induced impairments. *IEEE Trans. Aerosp. Electron. Syst.* 2002; **38**(3): 779-790.
7. F. Gargione, T. Iida, F.Valdoni and F. Vatalaro. Services, technologies, and systems at Ka band and beyond – A survey. *IEEE J. Sel. Areas Commun.* 1999; **17**(2):133-144.
8. A.F. Ismail, M.R. Islam, J. Din, A.R. Tharek and N.L.I. Jamaludin. Investigation of rain fading on a 26 GHz link in tropical climate. In *Proc. 6th Int. Conf. Telecommun. Syst., Services and Applicat.*. 2011, 126-129.
9. R.A. Farrugia and C.J. Debono. Accurate modeling of Ka-band videoconferencing systems based on the quality of experience. *IET Commun.* 2009; **3**(1): 67-74.
10. Q. W. Pan, J.E. Allnutt and C. Tsui. Evaluation of diversity and power control techniques for satellite communication systems in tropical and equatorial rain climates. *IEEE Trans. Antennas Propag.* 2008; **56**(10): 3293-3301.
11. C. Capsoni, M. D'Amico, R. Nebuloni and C. Riva. Performance of site diversity technique estimated from time diversity. In *Proc. 5th European Conf. Antennas and Propagation (EUCAP)*, 2011, 1463-1466.
12. J. X. Yeo, Y. H. Lee and J. T. Ong. Performance of site diversity investigated through radar derived results. *IEEE Trans. Antennas Propag.* 2011; **59**(10): 3890-3898.
13. Louis J. Ippolito Jr., Satellite Communications Systems Engineering: Atmospheric Effects, Satellite Link Design and System Performance. John Wiley and Sons, 2008.
14. R. Mathar and A. Schmeink. Proportional QoS adjustment for achieving feasible power allocation in CDMA systems. *IEEE Trans. Commun.* 2008; **56**(2):254-259.
15. I.M. Kim and H.M. Kim. Efficient power-management schemes for video service in CDMA systems. *IET Electron. Lett.* 2000; **36**(13): 1149-1150.
16. D. G. Sweeney and C. W. Bostian. Implementing adaptive power control as a 30/20-GHz fade countermeasure. *IEEE Trans. Antennas Propag.* 1999; **47**(1): 40-46.
17. H. Fukuchi and T. Saito. Novel mitigation technologies for rain attenuation in broadband satellite communication system using from Ka-to W-band. In *Proc. 6th Int. Conf. Inform. Commun. Signal Process.,* 2007, 1-5.
18. Y. Wang, J. Kang, Q. Chen, Qiang and M. Liu. Rain attenuation compensation scheme of the Ka band multi-beam satellite communication system. In *Proc. IET Int. Conf. Wireless, Mobile and Multimedia Networks*, 2006, 1-3.
19. Q. W. Pan, J. E. Allnutt and C. Tsui. Satellite-to-earth 12 GHz fade slope analysis at a tropical location. In *Proc. IEEE Antennas and Propag. Society Int. Symp.,* vol. 4A, 2005, 51-54.
20. M. Umehira, K. Kobayashi, Y. Yasui, M. Tanaka, R. Suzuki, H. Shinonaga and N. Kawai. Recent Japanese R&D in satellite communications. *IEICE Trans. Commun.* 2009; **E92-B** (11): 3290-3299.
21. Y. H. Lee, S. Winkler. Effects of rain attenuation on satellite video transmission. In *Proc. IEEE 73rd Conf. Veh. Technology (VTC Spring),* 2011, 1-5.
22. ITU-T, Coding of Audio-Visual Objects – Part 10: Advanced Video Coding, ITU-T Rec. H.264/ISO/IEC 14496-10:2012.
23. A. de Lattre, J. Bilien, A. Daoud, C. Stenac, A. Cellerier and J.-P. Saman. VideoLAN streaming howto. 2002-2005 the VideoLAN project. [Online]. Available: http://images1.videolan.org/doc/streaming-howto/en/streaming-howto-en.pdf
24. Tcpreplay. [Online]. Available: http://tcpreplay.synfin,net/trac/
25. M. Vranjes, S. Rimac-Drlje and D. Zagar. Subjective and objective quality evaluation of the H.264/AVC coded video. In *Proc. 15th Int. Conf. System, Signals and Image Processing (IWSSIP)*, 2008, 287-290.
26. A. K. Moorthy, K. Seshadrinathan, R. Soundararajan and A. C. Bovik. Wireless Video Quality Assessment: A Study of Subjective Scores and Objective Algorithms. *IEEE Trans. Circuits and Syst. Video Technol.*2010; **20**(4): 587-599.
27. S. Winkler and P. Mohandas. The Evolution of Video Quality Measurement: From PSNR to Hybrid Metrics. *IEEE Trans. Broadcast.* 2008; **54**(3): 660-668.
28. ITU-R, Propagation Data and Prediction Methods Required for the Design of Earth-Space Telecommunication Systems, ITU-R Rec. P.618-11, 2013.
29. ITU-R, Specific Attenuation Model for Rain for Use in Prediction Methods, ITU-R Rec. P.838-3, 2005.
30. A. Sharifi, K. Sabahi, M. A. Shoorehdeli, M. A. Nekoui and M. Teshnehlab. Load Frequency Control in Interconnected Power System using Multi-objective PID Controller. In *Proc. IEEE Conf. Soft Computing in Industrial Applications*, 2008, 217-221.
31. J. Sun and X. Liu. The Application Prospects of Intelligent PID Controller in Power Plant Process Control. In *Proc. Int. Conf. Modeling, Identification and Control*, 2012, 399-403.
32. D. Cavendish, M. Gerla, S. Mascolo. A Control Theoretical Approach to Congestion Control in Packet Networks. IEEE/ ACM Trans. Networking, 2004, **12**(5), 893–906,
33. G. Boggia, P. Camarda, L. A. Grieco, S. Mascolo. Feedback based control for providing real-time services with the 802.11e MAC, IEEE/ACM Trans. Networking, 2007, **15**(2), 323–333,
34. J. G. Ziegler and N. B. Nichols. Optimum Setting for Automatic Controllers. Transactions of the ASME, **115**(2B), 1993, 220-222.
35. E. Modiano, C. E. Rohrs. Power Allocation and Routing in Multibeam Satellites With Time-Varying Channels. IEEE/ACM Trans. Networking, 2003, **11**(1), 138-152.
36. Larry L. Peterson and Bruce S. Davie. *Computer Networks: A Systems Approach*. Morgan Kaufman, 2011,pp. 74-75.

37. N. Celandroni, E. Ferro, N. James, F. Potortì. FODA/IBEA-TDMA: A Flexible Fade Countermeasure System for Integrated Services in User-oriented Networks. Internat. J. Satell. Commun.,1992, **10**(6), 309–323.

Ting Ma received her BE degree from University of Electronic Science and Technology of China in 2009. She is currently working towards the Ph.D. degree in Electrical and Electronics Engineering from the Nanyang Technological University. Her research interests include satellite systems security and video streaming mechanisms.

Yee Hui Lee (S'96–M'02–SM'12) received the B.Eng. (Hons.) and M.Eng. degrees in electrical and electronics engineering from the Nanyang Technological University, Singapore, in 1996 and 1998, respectively, and the Ph.D. degree from the University of York, U.K., in 2002. She is currently Associate Professor and Assistant Chair (Student) of the School of Electrical and Electronic Engineering, Nanyang Technological University, where she has been a faculty member since 2002. Her interests are channel characterization, rain propagation, antenna design, electromagnetic bandgap structures, and evolutionary techniques.

Stefan Winkler is Principal Scientist and Director of the Interactive Digital Media Program at the University of Illinois' Advanced Digital Sciences Center (ADSC) in Singapore. He also serves as Scientific Advisor to Cheetah Technologies. Prior to that, he co-founded a start-up, worked in several large corporations, and held faculty positions at the National University of Singapore and the University of Lausanne, Switzerland.
Dr. Winkler has a Ph.D. degree from the Ecole Polytechnique Fédérale de Lausanne (EPFL), Switzerland, and an M.Eng./B.Eng. degree from the University of Technology Vienna, Austria. He has published over 90 papers and the book "Digital Video Quality." He is an Associate Editor of the IEEE Transactions on Image Processing and the IEEE Signal Processing Magazine (Standards Column), and a member of the IVMSP Technical Committee of the IEEE Signal Processing Society. He has also contributed to video quality standards in VQEG, ITU, ATIS, VSF, and SCTE. His research interests include video processing, computer vision, perception, and human-computer interaction.

Dr. Maode Ma received his BE degree from Tsinghua University in 1982, his ME degree from Tianjin University in 1991 and his Ph.D. degree in computer science from Hong Kong University of Science and Technology in 1999. Now, Dr. Ma is an Associate Professor in the School of Electrical and Electronic Engineering at Nanyang Technological University in Singapore. He has extensive research interests including wireless networking and network security. He has led and/or participated in around 20 research projects funded by government, industry, military and universities in various countries. He has been a member of the technical program committees for more than 130 international conferences. He has been a general chair, technical symposium chair, tutorial chair, publication chair, publicity chair and session chair for more than 50 international conferences. Dr. Ma has more than 220 international academic publications, including more than 90 journal papers and 130 conference papers. He currently serves as the Editor-in-Chief of *International Journal of Electronic Transport.* He also serves as a Senior Editor for *IEEE Communications Surveys and Tutorials*, and an Associate Editor for International *Journal of Network and Computer Applications,* International Journal of *Security and Communication Networks,* International Journal of *Wireless Communications and Mobile Computing* and *International Journal of Communication Systems.* He had been an Associate Editor for *IEEE Communications Letters* from 2003 to 2011. Dr. Ma is a senior member of *IEEE Communication Society and IEEE Education Society.* He is a member of the executive committee of the *IEEE Education Society*, Singapore Chapter. He is also a member of a few technical committees in the *IEEE Communication Society.*